2018 IEEE International Conference on Soft Robotics (RoboSoft)
Livorno, Italy, April 24-28, 2018

An Inverse Kinematics Method of a Soft Robotic Arm with Three-dimensional Locomotion for Underwater Manipulation

Zheyuan Gong [1], Jiahui Cheng [1], Kainan Hu [1], Tianmiao Wang [1,2] and Li Wen [1,2]*, *Member, IEEE*

***Abstract*—Soft robots have several promising features for underwater manipulation, e.g., safe interaction with surroundings, lightweight, low inertia, etc. In this paper, we proposed a method for the inverse kinematics of the soft manipulator that can move in the three-dimensional space. By controlling the two bending segments to move with opposing curvatures and one elongation segment to move up and down, our method enabled the real-time solution of the inverse kinematics and allowed the tip of the manipulator executing point-point movements in three dimensions. We performed the trajectory planning ability of the soft manipulator following the straight line and circle paths. Furthermore, we investigated the hydrodynamic functions of the soft manipulator underwater including forces, and the wake flows when the soft arm stroked at different amplitudes and frequencies. We found that the hydrodynamic force (<1N) and the torques (<0.1Nm) were quite small during locomotion-- which led to a negligible inertial impact on the underwater vehicle compared to the traditional rigid underwater manipulator. Finally, we demonstrated that the soft manipulator successfully picked and placed sea animals at 10m depth.**

I. Introduction

Recently, increasing studies on soft robotics have focused on the underwater applications by seeking bio-inspired ideas from aquatic animals. For example, the autonomous underwater soft robotic fish can excute both C-start and free-swimming locomotions [1]; the tissue engineered soft ray can be controlled to swim under external ultra-light [2]; the ionic polymer metal composite was applied to actuate as undulatory locomotion [3]; the multi-material 3D printed shark skin can enhance the self-propelled swimming speed [4][5]. For the grasping area, the structures, materials and actuation of the soft octopus arm has been studied extensively [6]; the eight soft arm robot can swim under wiggling locomotion of the arm [7], undersea grasping with soft squishy fingers was performed [9]; the liquid metal was embedded into the soft robotics to enable tunable mechanical degree of freedom, stiffness and sensing capacity [11]. For the underwater adhesion area, bio-inspired remora adhesive disc enable the underwater hitchhiking [8].

Among all biomimetic locomotion, underwater grasping and manipulation is an emerging field and important area that requires soft robotics technologies. The traditional rigid hydraulic robotic arms have large mass. The huge inertia caused by the rigid arm's movements would induce significant vibration for the underwater vihicle- which bring in big challenges to control the attitudes of the underwater vehicles during operating [21][22]. In contrast, soft arm manipulators have advantages of compliance and lightweight, and are promising for the underwater manipulation. To model the soft manipulator, the piecewise constant curvature (PCC) model has been developed [11] and was used for modeling of the bionic handling assistant [12], cable-driven soft manipulators [13] and soft elastomer arms [14][15], *etc*. A few works established models based on the geometrical information [12][15]. Researchers also applied neural networks for soft arms modeling [18], therefore to step over the complicated mathematical model and the non-linear material property.

To complement the complexity of the reverse kinematics of the soft, continuous robot [18]-[19], in this paper, we propose a novel method for the soft robotic manipulator's inverse kinematics that allows for real-time processing and requires less computing resources for controlling the 3D locomotion. Based on opposing curvatures of two bending segments with one elongation section, our method allows point-point movements in three-dimensional space and path planning to be realized. In addition, we investigate the hydrodynamic functions of the soft manipulator including forces, and the wake flows at different amplitudes and frequencies of the manipulator in a lab-based aquatic environment. Finally, we demonstrate underwater picking and placing tasks of the soft manipulator that was mounted on an underwater vehicle, showing the manipulation ability in the natural undersea environment.

II. Materials And Methods

A. Design

We designed and fabricated an entirely soft, underwater manipulator and soft gripper that can achieve movements in three dimensional space and performing grasping (figure 1(a)) [15][20]. The soft manipulator was 360mm in length (300mm for only the soft arm) and 34mm in diameter, with a mass of 322g. It was designed as a cylinder cross section to decrease the hydrodynamic resistance in the water flow. The soft manipulator consisted the four sections: two bending segments, one elongation segment, and one soft gripper (figure 1(b)). In each bending segment, we had three individual chambers. Meanwhile, it was covered with rubber tendons to reduce radial ballooning of the chambers when pressurizing (figure 1(c)). We applied the fiber-reinforced actuator on the elongation segments to grasp in different depth (figure 1(e)).

It should be noted that we actuated the soft manipulator in opposing curvature like "S" shape throughout the whole process. In opposing curvature, first, the two bending segments have the same curvature, which simplified the kinematic modeling; second, the soft gripper is always vertical to the ground which benefits grasping. We integrated two bending segments at an included angle of 180° (figure 1(c)). This design simplified the actuation of opposing curvature: if

This work was supported by the National Science Foundation supports key projects, China, under number 61633004 and 61333016. Authors are with the School of Mechanical Engineering and Automation [1], and Beijing Advanced Innovation Center for Biomedical Engineering [2], Beihang University, Beijing, 100191, People's Republic of China; *Please E-mail Prof. Li Wen for contact: liwen@buaa.edu.cn.

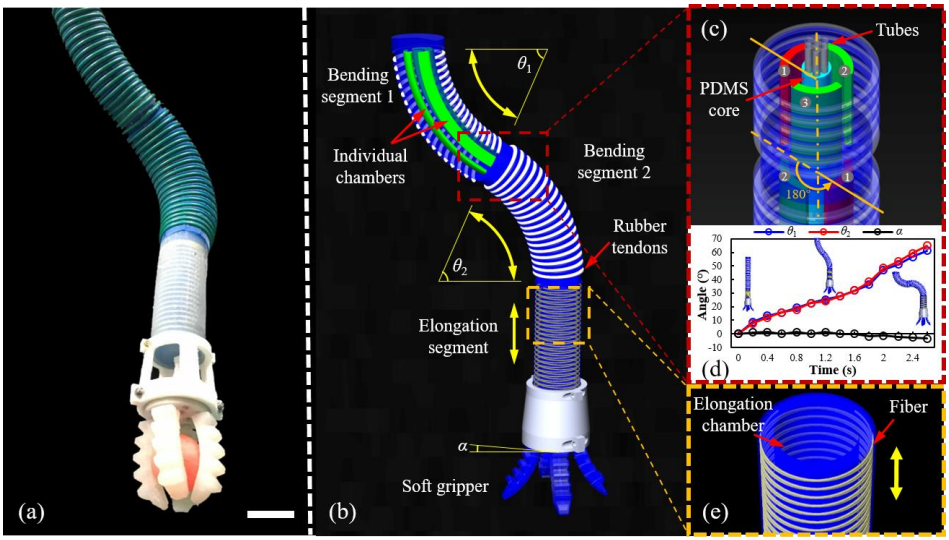

Figure 1. The design and movement principal of the soft manipulator. (a) The snapshot of the soft manipulator. Scale bar: 30mm. (b) The soft manipulator consisted of two bending segments, an elongation segment, and a soft gripper. (c) The inflating channels of two bending segments have an offset angle of 180. (d) The curvatures of bending segments 1 and 2 were actuated in opposing curvature. (e) The fiber-reinforced elongation segment.

only we actuated the opposite chambers in two segments, the soft manipulator always performed the opposing curved bending, no matter which direction it moved towards. Figure 1(d) showed the curve angles of two bending segments (θ_1, θ_2) and the intersection angle at the horizontal level of the soft manipulator tip (α) in one trial we actuated the soft manipulator. And we found that the θ_1, θ_2 were nearly the same and the α almost equaled zero, which the confirmed the design to realize opposing curvature.

B. Kinematics modeling

Figure 2(a) demonstrated the overview of the soft manipulator kinematics. The soft manipulator was always actuated in opposing curvature. The actuated conditions of opposite chambers were the same, and the curve angles of bending segments were always equal (θ_1=θ_2). Thus, the two bending segments shared the degrees of freedom (DOF) only had 2 DOF, while one bending segment had the DOF of the rotation φ and bending θ_1 (or θ_2). Due to the elongation segment, we could achieve three DOF movements and grasping.

Opposing curvature patterns offered plenty of advantages on kinematic modeling. First, the attitudes of two bending segments $\{\kappa_i, \varphi_i, \theta_i\}$ had very straightforward relationships (equations (4)(5)(6)). And we only needed to calculate the attitudes of one segments. Second, it reduced the number of inputs (seven independent chambers totally to four independent chambers). Thus, it reduced half of the computation contributed to the fast solution of kinematics.

The modeling procedure could be realized in two parts (figure 2(b)): (1) the transformation between the coordinates of the arm tip $\{x, y, z\}$ and chambers length $\{l_{i1}, l_{i2}, l_{i3}, l_e\}$ (l_{ij}, the indexes i and j mean segment i chamber j; l_e, the index e means the length of elongation segment; the same as below). The essential point of this part was how we could get an inverse solution from $\{x, y, z\}$ (three parameters) to $\{l_{i1}, l_{i2}, l_{i3}, l_e\}$ (four parameters) without other inputs. (2) The transformation between chambers length $\{l_{i1}, l_{i2}, l_{i3}, l_e\}$ and the pressure $\{p_{i1}, p_{i2}, p_{i3}, p_e\}$, the directly actuation parameter. By reason of the nonlinear response of soft material and complexity of structures, it was complicated to figure out (2) in a theoretical way, so we finished this work via experiments (figure 2(c)), and we fitted formulas for the model-based control recording these results. In order to simplify the model, we made assumptions as follow:

a) The bending section had the constant curvature rate, and the elongation section is totally straight. The curves were tangent at the intersection points.

b) The chambers in the same segment are parallel, and the cross sections are equal in the same section.

1) Forward Kinematics:

Previous works [11][15] had shown enough methods on how to solve the forward transformation questions. Combining these methods with the structures and sizes of our soft arm (shown in figure 2(d)), it's easy to get coordinates of the segments tip $\{x, y, z\}$ from the length of the chamber $\{l_{i1}, l_{i2}, l_{i3}, l_e\}$ with the help of attitudes $\{\kappa_i, \varphi_i, \theta_i\}$.

$$\kappa_1 = \frac{1}{r_1} = \frac{2\sqrt{l_{11}^2 + l_{12}^2 + l_{13}^2 - l_{11}l_{12} - l_{11}l_{13} - l_{12}l_{13}}}{(l_{11} + l_{12} + l_{13})d} \tag{1}$$

$$\varphi_1 = \tan^{-1}\left(\frac{l_{12} + l_{13} - 2l_{11}}{\sqrt{3}(l_{12} - l_{13})}\right) \tag{2}$$

$$\theta_1 = \frac{2\sqrt{l_{11}^2 + l_{12}^2 + l_{13}^2 - l_{11}l_{12} - l_{11}l_{13} - l_{12}l_{13}}}{3d} \tag{3}$$

In equations (1)(2)(3), d represented the radius of soft arm cross-section, and r_1 was the radius of the bending curve. Particularly, we used the surface length mainly considering it was more accessible for measurement. After we got the attitudes parameters from the bending segment 1, we could get attitudes of the other segment:

$$\kappa_2 = \kappa_1 \tag{4}$$

$$\varphi_2 = \varphi_1 + \pi \tag{5}$$

$$\theta_2 = \theta_1 \tag{6}$$

Furthermore, we could also get the coordinate of soft arm tip $\{x, y, z\}$ from the attitudes $\{\kappa_i, \varphi_i, \theta_i\}$ we got previously. Mathematically, we considered the soft manipulator simply

consisted of constant curvature curves (bending segments) and lines (elongation segments) based on the assumptions. The coordinate transformation in both curves and lines could be described by homogeneous matrixes shown in equation (7), where R is the rotation matrix, and p is the translation vector.

$$T=\begin{bmatrix} R & p \\ 0 & 1 \end{bmatrix} \tag{7}$$

Figure 2(d) showed the modeling of a single segment. We defined orientation angle φ_i represents the rotation angle around the z-axis, curvature angle θ_i represents the bending angle around the y-axis, where i indicates the ith segment. In the bending segments, we considered the bending procedure as: first the soft arm rotates around y-axis with angle θ_i; second, the soft arm rotates around z-axis with angle φ_i. Moreover, we needed to post-multiply the homogeneous matrix with the rotation matrix $R(-\varphi_i)$ and zero translation. The transformation matrix for the bending segment was demonstrated in equation (8) In elongation segments, we only needed to consider the translation on z-axis with a length of l_e (equation (9)).

$$\begin{aligned} {}^{i}_{i-1}T &= \begin{bmatrix} \mathrm{R}_z(\varphi_i) & 0 \\ 0 & 1 \end{bmatrix}\cdot\begin{bmatrix} \mathrm{R}_y(\theta_i) & p \\ 0 & 1 \end{bmatrix}\cdot\begin{bmatrix} \mathrm{R}_z(-\varphi_i) & 0 \\ 0 & 1 \end{bmatrix} \\ &= \begin{bmatrix} \cos^2\varphi_i\cos\theta_i+\sin^2\varphi_i & \cos\varphi_i\sin\varphi_i(\cos\theta_i-1) & \cos\varphi_i\sin\theta_i & r\cos\varphi_i(1-\cos\theta_i) \\ \cos\varphi_i\sin\varphi_i(\cos\theta_i-1) & \sin^2\varphi_i\cos\theta_i+\cos^2\varphi_i & \sin\varphi_i\sin\theta_i & r\sin\varphi_i(1-\cos\theta_i) \\ -\cos\varphi_i\sin\theta_i & -\sin\varphi_i\sin\theta_i & \cos\theta_i & r\sin\theta_i \\ 0 & 0 & 0 & 1 \end{bmatrix} \end{aligned} \tag{8}$$

$${}^{3}_{2}T=\begin{bmatrix} 1 & 0 & 0 & 0 \\ 0 & 1 & 0 & 0 \\ 0 & 0 & 1 & l_e \\ 0 & 0 & 0 & 1 \end{bmatrix} \tag{9}$$

Thus, we could get the forward transformation of the whole soft manipulator (equation (10)).

$${}^{3}_{0}T={}^{1}_{0}T\cdot{}^{2}_{1}T\cdot{}^{3}_{2}T \tag{10}$$

2) Inverse Kinematics:

Inverse kinematics is significant for the soft manipulator. With this capability, we could realize the coordinate based control and point to point movement of the soft manipulator. That's the foundation of the picking and placing tasks, as well as the trajectory planning and obstacle avoidance. Further, the quick solution of inverse kinematics also helps to improve the real-time control ability of soft manipulator. However, the inverse kinematics of soft robots (even continuum robots) was always a challenging problem [11]. The large group's nonlinear equations in the transformation matrix cause the huge complexity to the inverse solution. To our knowledge, how to figure out the quick inverse solution has not been reported.

We proposed a quick inverse solution on soft manipulators with the specific opposing curvature bending. As we discussed above that the soft manipulator had three DOF in coordinate space $\{x, y, z\}$. However, the soft manipulator had four independent chambers $\{l_{i1}, l_{i2}, l_{i3}, l_e\}$. In order to get the chambers length $\{l_{i1}, l_{i2}, l_{i3}, l_e\}$ (four outputs) from the coordinates $\{x, y, z\}$ (three inputs), we proposed a constraint condition: at most two chambers in a bending segment were actuated at the same time, so that at least one chamber in one bending segment was in initial length. Thus, the point of this method was to figure out which chamber was in initial length.

We also resolved the transformation from $\{x, y, z\}$ to $\{l_{i1}, l_{i2}, l_{i3}, l_e\}$ with the help of the attitudes $\{\kappa_i, \varphi_i, \theta_i\}$. First, we got the rotation angle φ_1 from the given inputs $\{x, y, z\}$.

$$\varphi_1=-\tan^{-1}\left(\frac{y}{x}\right) \tag{11}$$

Then we evaluated φ_1 to figure out which chamber was not actuated. The initial length of chambers could be pre-measured at the beginning. According to the geometry relationship in figure 2(e), we could give an equation where we represented the initial length with the attitudes parameters $\{\kappa_i, \varphi_i, \theta_i\}$. Here, on the relationship $\kappa_i=r_i^{-1}$, we also regarded r_i as attitudes parameter κ_i.

$$\begin{cases} l_{i1init}=\theta_1\cdot(r_1-d\sin\varphi_1), & \text{when } \dfrac{\pi}{6}\le\varphi_1<\dfrac{5\pi}{6} \\ l_{i2init}=\theta_1\cdot\left[r_1+d\cos\left(\varphi_1-\dfrac{\pi}{6}\right)\right], & \text{when } \dfrac{5\pi}{6}\le\varphi_1<\dfrac{3\pi}{2} \\ l_{i3init}=\theta_1\cdot\left[r_1-d\cos\left(\varphi_1+\dfrac{\pi}{6}\right)\right], & \text{when } \dfrac{3\pi}{2}\le\varphi_1<2\pi \text{ or } 0\le\varphi_1<\dfrac{\pi}{6} \end{cases} \tag{12}$$

Considering the geometry relationship shown in figure 2(d), we could propose another equation from the given coordinate:

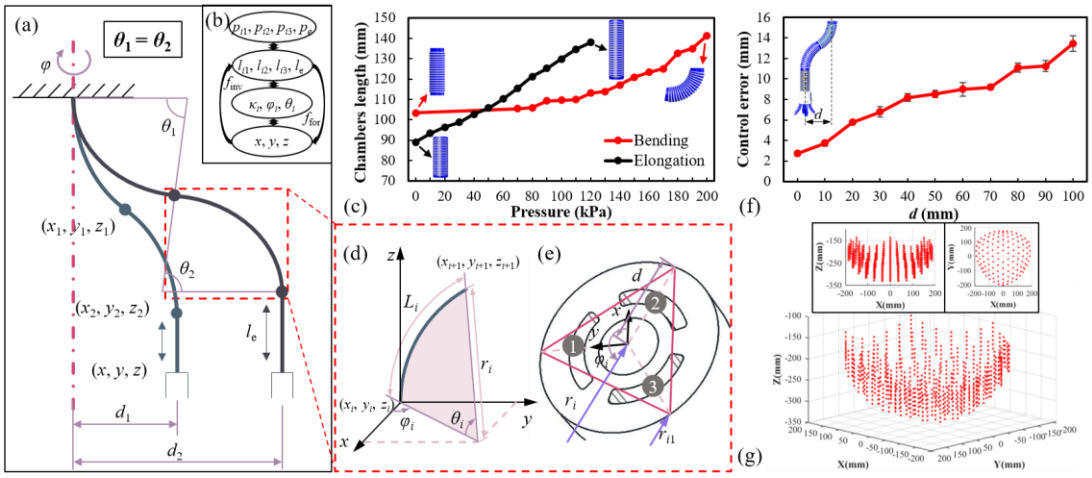

Figure 2. Kinematics modeling of the soft manipulator. (a) The bending segments of the soft manipulator was actuated in opposing curvature, i.e., the bending angles of bending segments were controlled to be equal (θ_1=θ_2). (b) The kinematic transformation map was demostrated as an inset. (c) Chambers length at different pressure was shown. (d) Geometrical functions of the bending segments. (e) Geometrical functions of the cross-section. (f) Control error at different operating radius under controlled peumatic pressure. (g) The simulation of operating workspace of the soft manipulator.

$$\frac{x}{2} = r_1 \cdot \cos\varphi_1 \cdot [1 - \cos\theta_1] \tag{13}$$

In equations (12) and (13), we could found that only r_1 and θ_1 were the unknown quantities. Combining the two equations, we could solve the rest attitudes parameters. Then, we easily got the length of all chambers $\{l_{i1}, l_{i2}, l_{i3}, l_e\}$.

$$\begin{cases} l_{i1} = \theta_i \cdot (r_i - d\sin\varphi_i) \\ l_{i2} = \theta_i \cdot \left[r_i + d\cos\left(\varphi_i - \frac{\pi}{6}\right) \right] \\ l_{i3} = \theta_i \cdot \left[r_i - d\cos\left(\varphi_i + \frac{\pi}{6}\right) \right] \\ l_e = -2r_1 \sin\theta_1 - z \end{cases} \tag{14}$$

Thus, we get specific inverse transformation from $\{x, y, z\}$ to $\{l_{i1}, l_{i2}, l_{i3}, l_e\}$. With the help of pressure – length calibration (figure 2(c)), we can transfer from $\{l_{i1}, l_{i2}, l_{i3}, l_e\}$ to the driving pressure $\{p_{i1}, p_{i2}, p_{i3}, p_e\}$ to finish the model-based control.

C. Experiments setup

1) Kinematic model based control

In order to evaluate the capability of the kinematic model, we performed experiments on the model based location error and trajectory planning. We applied a stereo cameras system to capture the position of the soft manipulator in different motions and trajectories. The soft manipulator was mounted in water and actuated by seven proportional valves (ITV0030, *SMC*, Japan). The stereo cameras was carefully calibritated, and the error was less than 0.5mm. Moreover, we rebuilt the motions and got the coordinates of marker points from the images of different views. We performed the location error in different directions (φ_i) with the distance (d) ranging from 0mm to 100mm, 10mm of step length. We also performed the trajectory planning ability with paths of line and circle. Then, we ran the workspace simulation in MATLAB.

2) Hydrodynamics

To examine how much force and torque the soft manipulator generated underwater, and what the water flowed like when the soft manipulator was moving, we set up a hydrodynamic investigation platform (figure 4(a)). To avoid the interference effect of the tank surface, we mounted the soft manipulator at mid-depth of the water tank. We applied a six-axis force transducer (mini-40, *ATI*, Canada) measuring the hydrodynamic forces. In the DPIV (Digital Particle Image Velocimetry) experiments, a high-speed camera (SP-5000, *JAI*, Denmark) was used to record images of water flow at a frequency of 250 Hz. We obtained the velocity by processing of the images. The soft manipulator was programmed to move in a I-shaped stroke with different amplitudes A (50mm, 100mm, 150mm, 200mm) at different frequencies f (0.3Hz, 0.4Hz, 0.5Hz). When A=120mm, f=0.5Hz, we captured the flow fields to examine how soft manipulator impacted the flow field when picking and placing in the water tank.

III. Results And Discussion

A. Kinematic model based control (control error and trajectory planning) and workspace simulation

The soft manipulator was actuated at different distances (d) in several directions (φ_i), and the average control errors were demonstrated in figure 2(f). We found that the control error stayed in the range of 2.7~13.4mm with the distances changing from 0mm to 100mm. This error range was in error tolerance area of the soft gripper (the deviation of gripper and objects that the gripper could still grasp successfully, which has been demonstrated in our previous works [16][17]). These results indicated that the soft manipulator performed a controllable capability when doing pick and place tasks at exact points. According to the kinematic model, simulation on the workspace of the soft arm was illustrated as figure 2(g). The results showed that the soft manipulator collected a plate-shaped workspace with the size of approximately 400mm diameter and 100mm height.

Further, we demonstrated the trajectory planning ability of the soft manipulator with paths of line and circle (figure 3). In the line trajectory, the soft manipulator was actuated from the point A(-110, -64, -270) (unit: mm, the same in following coordinates) to the point B(110, 64, -295) at a constant speed of 32mm/s. The red circles were tracked points from the experiments, the blue line was the desired path that we programmed on a computer, the black lines represented the soft manipulator, and the black dots on the black lines represented the intersections of different segments. The results showed that experiment trajectory had a very little deviation from the desired path in 3D space. At 0~6s (former 85% distance), the tracked points matched the programmed path well and the error was less than 6.6mm in this time range (figure 3(b)). After 6s (last 15% distance), the soft manipulator reached the B point with a 2 seconds delay. In the circle trajectory, the soft manipulator was actuated from the point A(-55, -35, -285) to the point B(55, 35, -320) with a rotation angle

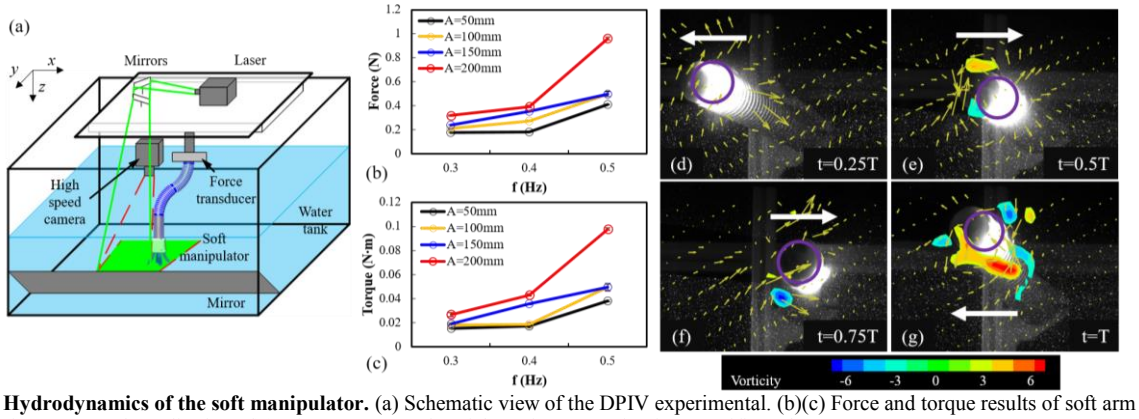

Figure 3. Hydrodynamics of the soft manipulator. (a) Schematic view of the DPIV experimental. (b)(c) Force and torque results of soft arm actuated at different frequency and amplitudes. (d)(e)(f)(g) DPIV results of the soft arm moving in a specific path.

of 120°, radius of 65mm and speed of 45mm/s, shown in figure 3(c). In time range, it had a vibration that might be related to the sudden change of moving directions. These results showed the capability that the soft manipulator following a specific trajectory. Lines and circles are the fundamental path shapes, and we can further achieve more complex trajectory tracking integrating lines and circle.

The inverse kinematics of soft robots (even continuum robots) was a challenging problem [11]. To solve this problem, Jiang *et al*. [18] applied neural network to determine optimal inverse kinematics. Lakhal *et al*. applied Sequential Quadratic Program on inverse kinematic modeling [19]. However, these methods needed huge computation resources. To our knowledge, the quick inverse solution has not been reported. We proposed a simple but quick and universal inverse solution for the soft manipulators whose structure and actuation were followed the opposing curvature. Further, we accomplished the location control of the soft manipulator on this method. And the control error was less than 13.4mm in its workspace. This method also contributed to the real time control. The inverse kinematics enabled the soft manipulator to follow trajectories (line and circle) and achieve a good dynamic response. The inverse solution was quick enough to provide the real-time actuation parameters for every subdivision on path. Thus, the soft manipulator achieved the ability to position and track complicated trajectories.

B. Hydrodynamics of underwater operation

Figure 4(b)(c) indicated how force and torque changed with frequency and amplitudes. In each trial of three repeats, the force and torque were defined as the peak value of raw data. Notably, when the soft manipulator moved at the amplitude of 50mm, the force increased from 0.178N to 0.409N (229.7%) when the frequency increased. The force at 100mm and 150mm remained similar to that of 50mm. However, the growth of 200mm, which increased to 0.960N when the frequency was 0.5Hz, was far faster than those at the other three amplitudes. As for torques (figure 4(c)), the torque at 200mm was significantly larger than those at 50mm, 100mm, and 150mm. When the amplitude was 50mm, the torque had a minor increment from 0.015N·m to 0.037N·m (250.1%). Enlarging frequency to 0.5Hz, the torque of 200mm was 0.097N·m, 2.55 times stronger than those of 0.3Hz. The results above proved that our soft manipulator could perform picking and placing tasks under a promising amplitude less 150mm. Figure 4(d) showed the result of PIV experiments of the soft manipulator. At 120mm and 0.5Hz in still water, we captured the water flow at 0.25T, 0.5T, 0.75T and 1T (T was the undulation period). The vortex structure was similar to the typical flow around a circular cylinder. In 1T, with time and moving distance accumulated, the vortexes behind the soft arm were enhanced and formed the Karman Vortex Street.

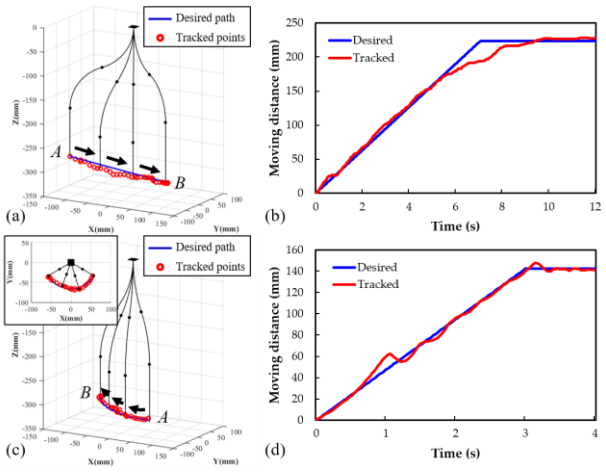

Figure 4. Trajectories of the line (a) and circle (c). Dynamic response while tracking (b) the line trajectory and (d) the circle trajectory.

Rigid robotic arms and grippers for the underwater manipulations have a huge mass and inertia which impacts their maneuverability. Soft robots have advantages of compliance and lightweight and may play an important role in underwater manipulation. However, no study has quantified the hydrodynamics of soft manipulators. We performed the hydrodynamics with the entirely soft manipulator for the first time. Compared with the rigid hydraulic manipulators, our soft manipulator had exceptional features of lightweight and low inertia. 1) Lightweight: the soft manipulator had a mass of 0.322kg (almost zero mass in water), while with a length of 360mm. The current prototype was significantly lighter than the traditional rigid hydraulic manipulators that commonly had a mass of tens of kilograms, *e.g.* a hydraulic manipulator with a length of 499mm had a total mass of 17.2kg [21]. 2) Low inertia: the soft manipulator under a 0.5Hz (frequency) and 200mm (amplitude) stroke generated a hydrodynamic force of 0.960N and torque of 0.097N·m. In contrast, a 695mm, 3.25kg rigid underwater arm generated 50N force and 15N·m torque when moving at 0.18Hz [22]. Thus, locomotion of the soft manipulator had negligible inertial effect for the underwater vehicle than the traditional rigid underwater manipulator. However, the soft manipulator also had low stiffness, slow response and back drivability. We could further improve these via hydrodynamics analysis and close-loop control.

C. Field test of underwater manipulation and grasping

To examine the capabilities of our underwater soft manipulator, we integrated it with a 3-DOF underwater vehicle for the underwater field test (figure 5(a)). We performed the manipulation by grasping marine seafood animals (sea cucumbers, echini, *etc*.) in the natural undersea environment. The undersea grasping was realized in three steps: 1) The underwater robot approached the targets area and hovered at that position. 2) The soft manipulator was actuated to approach the undersea animals with the gripper buckling. 3) The soft manipulator picked the target and placed it into a collecting basket. Both the soft manipulator and underwater robot were under remote control via the real-time underwater camera. In consequence, we successfully grasped echini (figure 5(b)) and sea cucumbers (figure 5(c)) at the depth 10m undersea.

Galloway *et al*. applied a rigid hydraulic arm with soft robotic squishy fingers, and demonstrated successful grasping of sea reefs [9]. In this paper, we performed that the soft manipulation could grasp sea animals (sea cucumbers, echini, *etc*.) in the natural, unstructured undersea environment. In the 10m depth undersea, our soft manipulator showed flexible motions. It was purely soft and had the ability to interact with fragile organisms like the sea cucumbers without any damage. It also could grasp irregularly shaped animals like echini. The compliance also benefited the mission success rate, which we achieved more than 80% of succession rate of undersea grasping. The soft-bodied manipulator also had the natural resistance to huge collision. Our results showed that the soft

manipulator has inherent advantages of compliance and is promising for the future underwater manipulation.

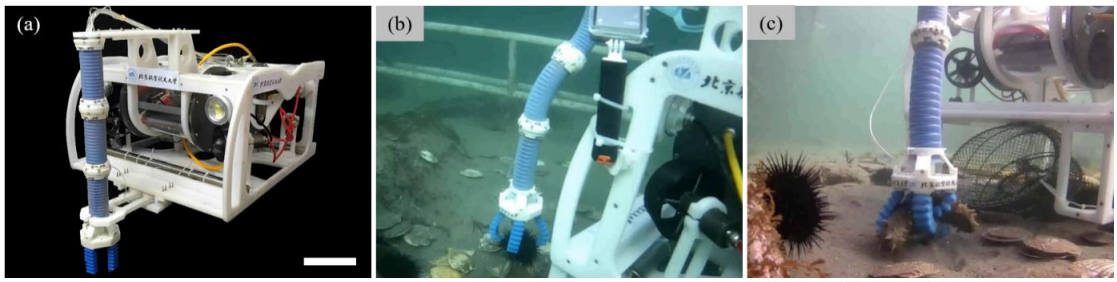

Figure 5. Undersea grasping with the soft manipulator mounted on an underwater robot. (a) The overall image of the underwater robot. The length of scale bar is 100mm. (b)(c) grasping undersea animals (echini and sea cucumbers) with soft manipulator at 10m undersea.

IV. CONCLUSION

In this paper, we proposed a novel inverse kinematics of a soft manipulator for underwater grasping. The soft manipulator was actuated in opposing curvature bending and could achieve three-dimensional movements in free space. We performed a simple but useful inverse solution for opposing curvature bending motion. This method required less computing resources and successfully controlled the position of the soft manipulater. The results showed that control error was less than 13.4mm. We also performed the trajectory planning ability of the soft manipulator by following the paths of a straight line and a circle. The experimental tracking points fitted the desired position well in both positions and time scale. Further, we investigated the hydrodynamic functions of the soft manipulator including forces, and the wake flows when moving at different amplitudes and frequencies. Surprisingly, we found that the magnitudes of the hydrodynamic force (<1N) and the torques (<0.1Nm) were quite small -- which led to a negligible inertial effect for the underwater vehicle compared to traditional rigid underwater manipulators. Finally, we performed the field test—we tested the manipulation capacity of soft arm in the natural undersea environment. The soft arm manipulator successfully grasped sea animals at a sea depth of 10m on a underwater robot. This showed the potential application that soft manipulators could be used in the underwater manipulation. For the future work, close-loop control of the soft manipulator with sensory feedback will be investigated.

REFERENCES

[1] Marcheseandrew, D, D. Onalcagdas, and Rus Daniela. "Autonomous Soft Robotic Fish Capable of Escape Maneuvers Using Fluidic Elastomer Actuators." *Soft Robotics* 1.1(2014):75.

[2] Park S J, Gazzola M, Park K S, *et al*. "Phototactic guidance of a tissue-engineered soft-robotic ray". *Science*, 2016, 353(6295):158.

[3] Shen, Qi, *et al*. "Hydrodynamic performance of a biomimetic robotic swimmer actuated by ionic polymer-metal composite." *Smart Materials & Structures* 22.7(2013):075035.

[4] Wen, L., J. C. Weaver, and G. V. Lauder. "Biomimetic shark skin: design, fabrication and hydrodynamic function." *Journal of Experimental Biology* 217.Pt 10(2014):1656.

[5] Wen L, Weaver J C, Thornycroft P J, *et al*. "Hydrodynamic function of biomimetic shark skin: effect of denticle pattern and spacing". *Bioinspiration & Biomimetics*, 2015, 10(6):066010.

[6] Calisti M, Giorelli M, Levy G, Mazzolai B, Hochner B, Laschi C, Dario P. "An octopus-bioinspired solution to movement and manipulation for soft robots," *Bioinspiration & Biomimetics*, 2011, 6:525-531.

[7] Cianchetti, M, *et al*. "Bioinspired locomotion and grasping in water: the soft eight-arm OCTOPUS robot." *Bioinspiration & Biomimetics* 10.3(2015):035003.

[8] Wang Y, Yang X, Chen Y, Wainwright D K, Kenaley C P, Gong Z, Liu Z, Liu H, Guan J, Wang T, Waver J C, Wood R J, and Wen L. "A biorobotic adhesive disc for underwater hitchhiking inspired by the remora suckerfish", *Science Robotics*, 2017, 2(10):8072.

[9] Galloway, K. C., *et al*. "Soft Robotic Grippers for Biological Sampling on Deep Reefs." *Soft Robotics* 3.1(2016):23.

[10] Hao Y, Wang T, Xie Z, *et al*. "A eutectic-alloy-infused soft actuator with sensing, tunable degrees of freedom, and stiffness properties." Journal of Micromechanics and Microengineering. DOI: 10.1088(2017).

[11] Webster Iii, Robert J, and B. A. Jones. "Design and Kinematic Modeling of Constant Curvature Continuum Robots: A Review." *International Journal of Robotics Research* 29.13(2010):1661-1683.

[12] Rolf, Matthias, and J. J. Steil. "Constant curvature continuum kinematics as fast approximate model for the Bionic Handling Assistant." *Ieee/rsj International Conference on Intelligent Robots and Systems* IEEE, 2012:3440-3446.

[13] Wang, Hesheng, *et al*. "Visual servo control of cable-driven soft robotic manipulator." *Ieee/rsj International Conference on Intelligent Robots and Systems* IEEE, 2013:57-62.

[14] Marchese, A. D., and D. Rus. "Design, kinematics, and control of a soft spatial fluidic elastomer manipulator." *International Journal of Robotics Research* 35.7(2015).

[15] Gong, Zheyuan, *et al*. "Design, fabrication and kinematic modeling of a 3D-motion soft robotic arm." *IEEE International Conference on Robotics and Biomimetics* IEEE, 2017:509-514.

[16] Hao, Yufei, *et al*. "Universal soft pneumatic robotic gripper with variable effective length." *Control Conference* IEEE, 2016:6109-6114.

[17] Hao, Yufei, *et al*. "Modeling and experiments of a soft robotic gripper in amphibious environments." *International Journal of Advanced Robotic Systems.* 14.3(2017):172988141770714.

[18] Jiang, Hao, *et al*. "A two-level approach for solving the inverse kinematics of an extensible soft arm considering viscoelastic behavior." *IEEE International Conference on Robotics and Automation*, 2017.

[19] Lakhal, Othman, *et al*. "Inverse Kinematic modeling of a class of continuum bionic handling arm." *Ieee/asme International Conference on Advanced Intelligent Mechatronics IEEE,* 2014:1337-1342.

[20] Martinez, Ramses V, et al. "Robotic Tentacles with Three-Dimensional Mobility Based on Flexible Elastomers." *Advanced Materials* 25.2(2013):205-212.

[21] Fernandez J J, Prats M, Sanz P J, *et al*. Grasping for the Seabed: Developing a New Underwater Robot Arm for Shallow-Water Intervention[J]. *IEEE Robotics & Automation Magazine*, 2013, 20(4):121-130.

[22] Takahashi, Akemi, and M. Nakashima. "Clarification of Unsteady Fluid Force Acting on Limbs in Swimming Using an Underwater Robot Arm: Development of an Underwater Robot Arm and Measurement of Fluid Force(Fluids Engineering)." *Journal of Fluid Science & Technology* 7.1(2012):114-128.